

**Zircon petrochronology reveals the distinct and linked tectono-magmatism of the  
Proto- and Paleo-Tethys orogenic cycles**

Bin Zhang<sup>a, b, \*</sup>, Wen Chen<sup>a, \*</sup>, Zhi-Liang Zhang<sup>c, \*</sup>, Zhi-Hao Sun<sup>b, d</sup>, Jing Yang<sup>e</sup>, Ze-Yang  
Zhu<sup>b</sup>, Jia-Qi Liu<sup>b</sup>

<sup>a</sup> Laboratory of Isotope Thermochronology, Institute of Geology, Chinese Academy of Geological Sciences,  
Beijing 100037, China

<sup>b</sup> Key Laboratory of Cenozoic Geology and Environment, Institute of Geology and Geophysics, Chinese  
Academy of Sciences, Beijing 100029, China

<sup>c</sup> Institute of Geology, China Earthquake Administration, Beijing 10029, China

<sup>d</sup> University of Chinese Academy of Sciences, Beijing 100049, China

<sup>e</sup> Institute of Geomechanics, Chinese Academy of Geological Sciences, Beijing 100081, China

**Contents of this file**

Texts S1-S2  
Figures S1-S3  
Tables S1

**Additional Supporting Information (Files uploaded separately)**

Dataset S1: The raw and reduced data of zircon U-Pb isotopic and trace elements.

**Introduction**

- Text S1: Zircon U-Pb isotopic and trace elements analytical methods, and data reduction
- Text S2: Zircon classification and crustal thickness, zircon Ti-saturation temperature and oxygen fugacity calculation
- Figure S1: Zircon U-Pb ages of bedrocks in the WKOB
- Figure S2: Detailed zircon U-Pb ages pattern
- Figure S3: Zircon classification
- Table S1: River sand sample locations

**Text S1.** Zircon U-Pb isotopic and trace elements analytical methods, and data reduction

Detrital zircons were separated using conventional magnetic and heavy liquid techniques. ~500 grains were randomly handpicked from each sand sample under a microscope to minimize sampling bias. The selected zircons were mounted in epoxy resin discs, polished to expose their interior structure, and ultrasonically cleaned in ultrapure water. Transmitted, and reflected light microscopy, along with cathodoluminescence (CL) imaging were employed to elucidate the interior structures and morphological features. CL analyses were performed at Beijing GeoAnalysis Co. Ltd. using a JEOL IT-500 scanning electron microscope (SEM) equipped with a DELMIC CL system. Operating parameters included a 10 kV acceleration voltage, 16.7 mm working distance, 63 nA probe current, and 12  $\mu$ s dwell time.

Zircons exhibiting magmatic oscillatory zoning were selected for U-Pb isotopic and trace elements analyses, conducted at two institutions. At Beijing GeoAnalysis Co. Ltd., WKL21-prefixed samples were analyzed using an Agilent 7900 ICP-MS coupled with a NWR193UC laser ablation system, operating at 6 Hz with a 30  $\mu$ m spot diameter and 5 J/cm<sup>2</sup> energy density. WKL22-prefixed samples were analyzed at the Institute of Geomechanics, Chinese Academy of Geological Sciences, utilizing an identical ICP-MS paired with a 193 nm GeoLas HD ArF excimer laser ablation system, operating at 5 Hz with a 32  $\mu$ m spot diameter and 5 J/cm<sup>2</sup> energy density.

Signal integration times were set to ~25 seconds for background and ~45 seconds for sample measurements. Data reduction was performed using *lolyte4* software (Paton et al., 2011). For U-Pb geochronology, zircon standards 91500 or GJ-1 served as external calibrants, while Plesovice zircon was analyzed as a quality monitor (Table S). Downhole fractionation was corrected using the exponential function method (Paton et al., 2011). Age concordance was defined using the perpendicular log ratio distance to the concordia line (Vermeesch, 2021), and only analyses with less than 10% discordance were considered for interpretation. Trace elements concentrations were processed using NIST SRM 610 as the external standard and <sup>29</sup>Si as the internal standard, with NIST SRM 612 analyzed as a quality control reference material.

**Text S2.** Zircon classification and crustal thickness, zircon Ti-saturation temperature and oxygen fugacity calculation

Granitoids, the primary source of zircons, are classified as I-type or S-type according to the proportion of sediments in the source region (Chappell & White, 2001; Li et al., 2021; Zhu et al., 2020). S-type granitic magmas primarily form through partial melting of upper-middle crustal metasediments, particularly turbidites, and represent a minor proportion of granites. In contrast, I-type granitic magmas, also contributed by minor sediments, originate from deeper crustal sources (Li et al., 2021; Zhu et al., 2020). Given that the apatite readily dissolves in S-type granitic melts, increasing effective P content. This phosphorus, along with trivalent rare earth elements and  $Y^{3+}$ , substitutes for  $Zr^{4+}$  and  $Si^{4+}$  in zircon, resulting in elevated P concentrations (Hoskin & Schaltegger, 2003). Thus, the molar concentration of P and REE+Y ( $\mu\text{mol/g}$ ) in zircon serves as effective discriminators between I-type and S-type granitic sources (Burnham & Berry, 2017; Zhu et al., 2020).

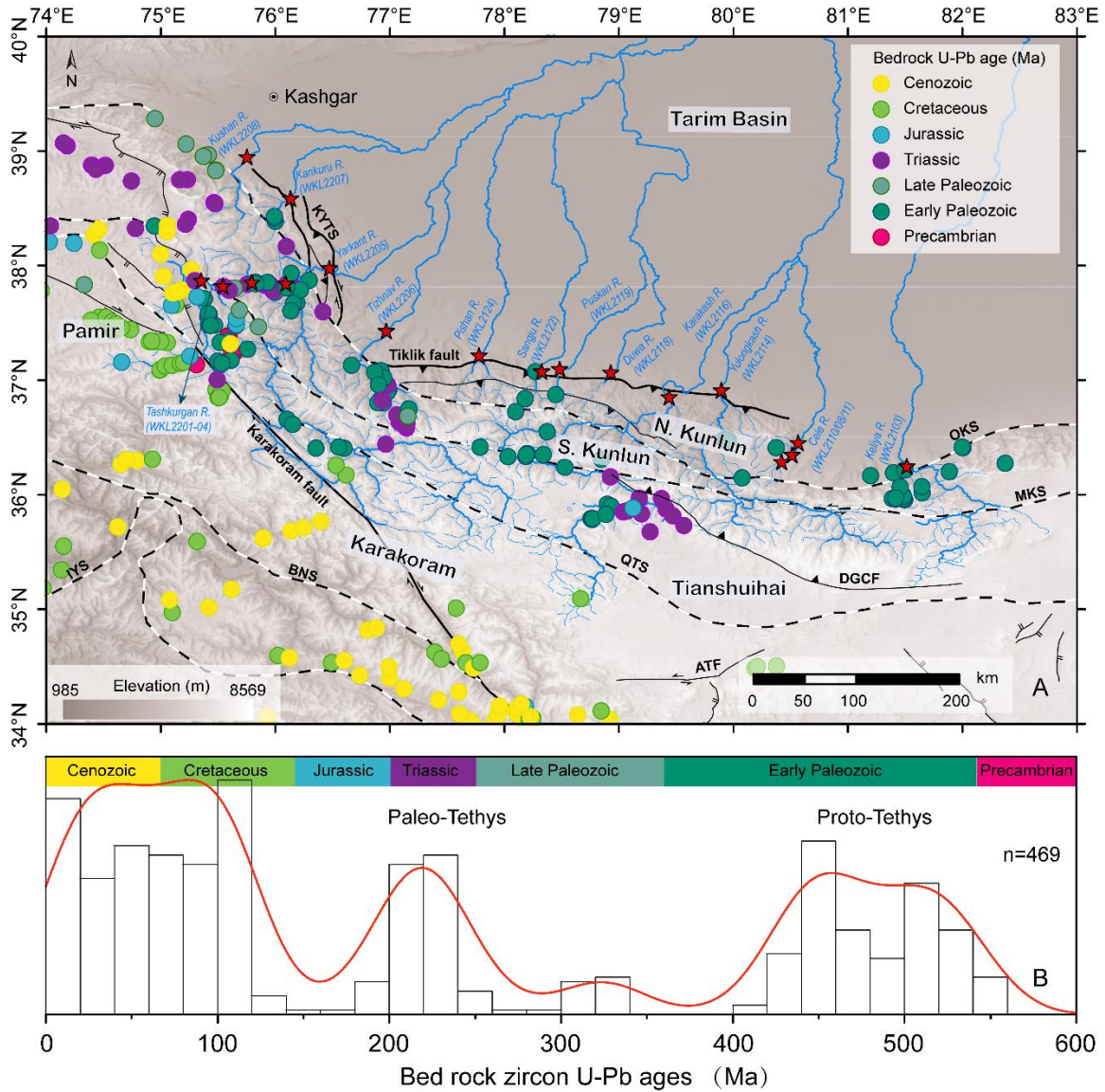
High-pressure conditions during crustal thickening inhibit plagioclase growth and prevent Eu depletion in the melt. Under these conditions, stable garnet preferentially incorporates  $Fe^{2+}$  from the melt, increasing  $Fe^{3+}/\Sigma Fe$  ratio and oxidization state. This promotes the conversion of  $Eu^{2+}$  to  $Eu^{3+}$ , enhancing  $Eu^{3+}$  partitioning in zircon. In contrast, plagioclase is only stable at shallow crustal levels under low-pressure conditions, incorporates  $Eu^{2+}$  due to its similar properties to  $Sr^{2+}$  and  $Ca^{2+}$ , depleting Eu in residual melts. Furthermore, the oxygen state of felsic magma correlate with differentiation pressure (Tang et al., 2020 with references therein). Meanwhile, during weathering, Sr leaching from plagioclase and produce Sr-depleted clay minerals which are important source materials for S-type granite (Chappell & White, 2001; Liu et al., 2022). Therefore, only I-type zircon  $Eu/Eu^*$  ratios [chondrite normalized  $Eu/(Sm \times Gd)^{1/2}$ ] serves as reliable indicator of magmatic differentiation pressure, and reconstruct the paleo crustal thickness based on the formula:  $z = (84.2 \pm 9.2) \times Eu/Eu^* + (24.5 \pm 3.3)$  (Tang et al., 2020).

$ZrSiO_4$ ,  $ZrTiO_4$  and  $TiSiO_4$  function as independent variable phase components in zircon. Due to their similar ionic radii,  $Ti^{4+}$  readily substitutes for  $Zr^{4+}$  in the zircon crystal lattice. The solubility of Ti in zircon strongly depends on temperature and is influenced by the activities of  $TiO_2$  ( $a_{TiO_2}$ ) and  $SiO_2$  ( $a_{SiO_2}$ ) (Ferry & Watson, 2007 with references therein).

This relationship forms the basis of the Ti-saturation thermometer, i.e.,  $T = \frac{4800 \pm 86}{5.711 \pm 0.072 - \lg(Ti) - \lg(a_{SiO_2}) + \lg(a_{TiO_2})} - 273.15$  (Ferry & Watson, 2007), which can determine zircon crystallization temperatures. In intermediate-felsic rocks, where zircon coexists with quartz,  $a_{SiO_2}$  is assumed to be 1. While  $a_{TiO_2}$  is assumed to be 0.8, this value is difficult to constrain for detrital zircons from diverse settings and may introduce temperature uncertainties of ~30-40 ° C (Ferry & Watson, 2007).

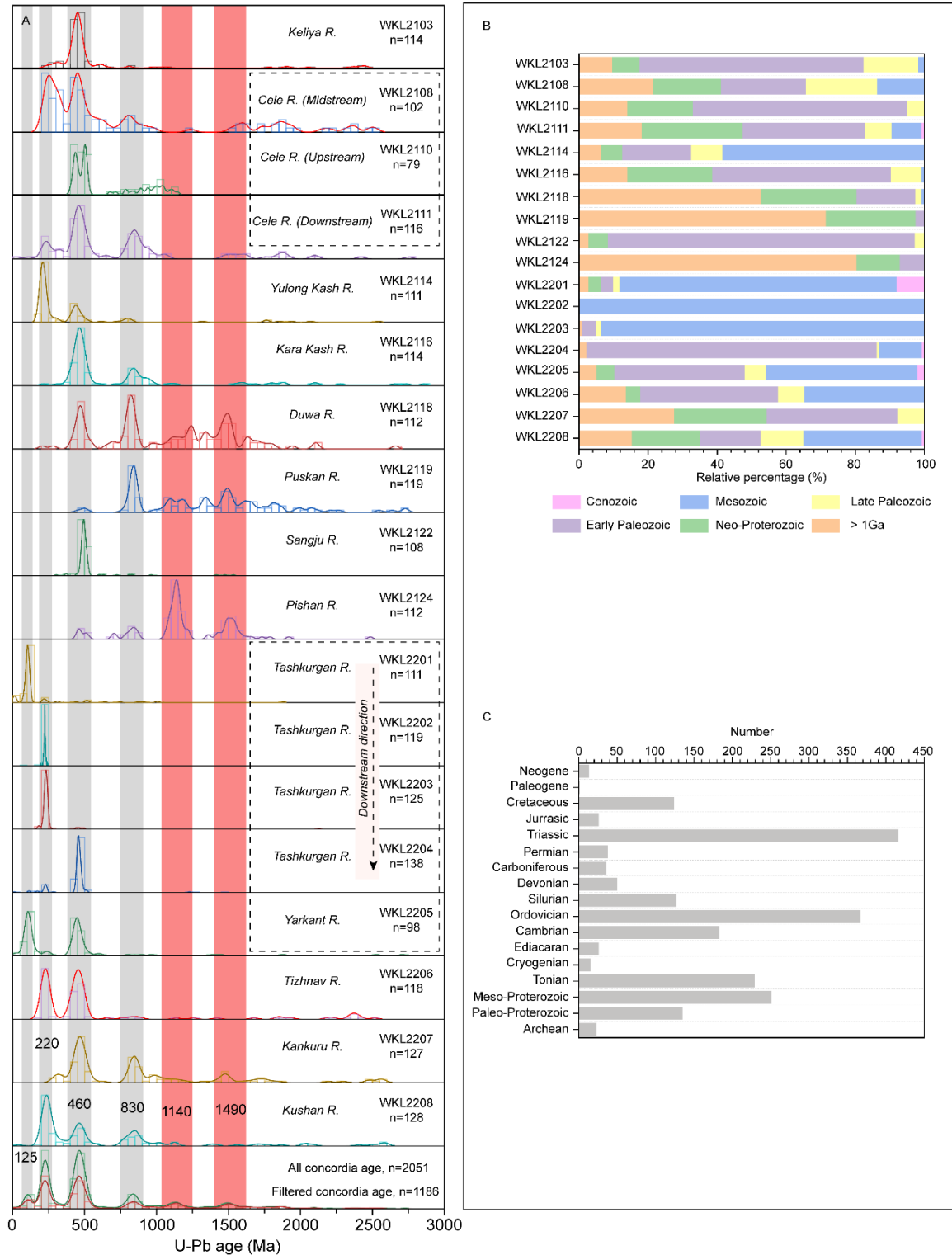
Oxygen fugacity reflects the redox state during magma crystallization and is typically expressed in logarithmic units relative to  $\Delta FMQ$  (Fayalite-Magnetite-Quartz buffer).  $Ce^{4+}$  and  $U^{4+}$  share identical ionic radii and coordination geometry in both aluminosilicate melts and zircon. However, their zircon/melt partition coefficients respond oppositely to the changes in oxygen fugacity. Consequently, magmatic oxidation state during zircon crystallization can be determined using zircon Ce/U ratios, with Ti content serving as an index of magmatic differentiation (Loucks et al., 2020). This Ce-U-Ti oxybarometer, empirically calibrated and independent of ionic charge, crystallization temperature, pressure, and host rock composition, is particularly suitable for analyzing detrital zircons (Loucks et al., 2020).

**Figure S1.** Zircon U-Pb ages of igneous bedrocks in the WKOB\*



\* The source data was compiled by (Xiang et al., 2023). Figure S1B contains 249 Cretaceous-Cenozoic U-Pb ages in the Pamir (related to the Neo-Tethys), which areas beyond the scope of Figure S1A. OKS: Oyttag-Kudi Suture; MKS: Mazar-Kangxiwa Suture; QTS: Qiaoertianshan Suture; BNS: Bangong-Nujiang Suture; DGCF: Dahongliutan-Guozha Co fault; IYS: Indus-Yarlung Suture; KYTS: Kashgar-Yecheng transfer system

**Figure S2.** Detailed zircon U-Pb ages pattern\*



(A) Histograms and Kernel density estimate curves of each sample's zircon concordant U-Pb ages. (B) Age constitution of each sample. (C) Age constitution of the total detrital zircon grains (n=2051).

**Figure S3.** Zircon classification based on the relationship between P and REE+Y ( $\mu\text{mol/g}$ )

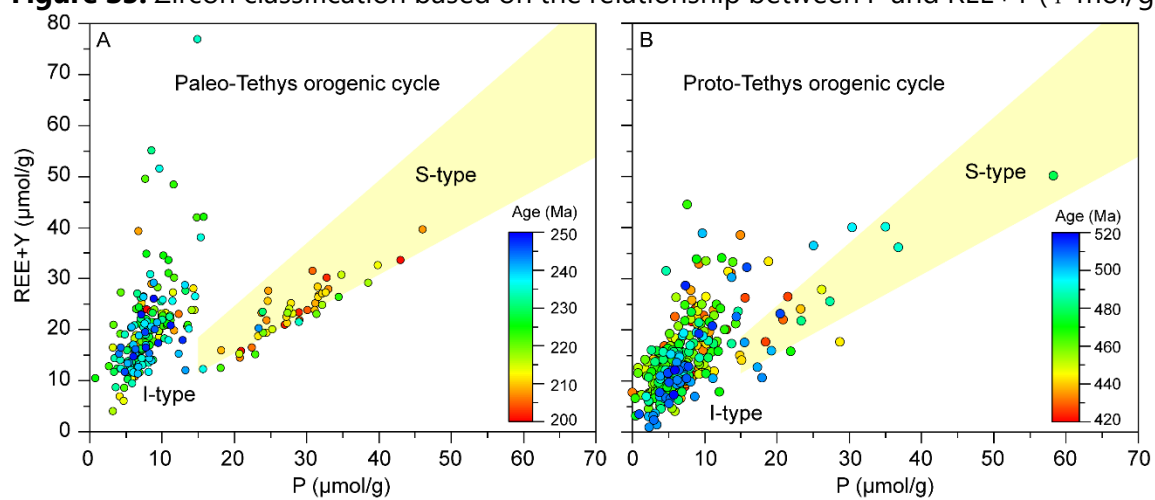


**Table S1.** River sand sample locations.

Sample No.	River name	Longitude (E)	Latitude (N)
WKL2103	Keliya	81.5168	36.2463
WKL2108	Cele	80.5140	36.3459
WKL2110	Cele	80.4232	36.2860
WKL2111	Cele	80.5672	36.4518
WKL2114	Yulong Kash	79.8962	36.9115
WKL2116	Kara Kash	79.4408	36.8514
WKL2118	Duwa	78.9312	37.0658
WKL2119	Puskan	78.4853	37.0963
WKL2122	Sangju	78.3273	37.0764
WKL2124	Pishan	77.7813	37.2146
WKL2201	Tashkurgan	75.3560	37.8687
WKL2202	Tashkurgan	75.5446	37.8201
WKL2203	Tashkurgan	75.7974	37.8524
WKL2204	Tashkurgan	76.0947	37.8426
WKL2205	Yarkant	76.4749	37.9768
WKL2206	Tizhnav	76.9712	37.4292
WKL2207	Kankuru	76.1353	38.5857
WKL2208	Kushan	75.7556	38.9479

**Data Set S1.** The raw and reduced data of zircon U-Pb isotopic and trace elements (upload separately in xlsx format).



## References

- Burnham, A. D., & Berry, A. J. (2017). Formation of hadean granites by melting of igneous crust. *Nature Geoscience*, 10(6), 457-461. <https://doi.org/10.1038/ngeo2942>
- Chappell, B. W., & White, A. J. R. (2001). Two contrasting granite types; 25 years later. *Australian Journal of Earth Sciences*, 48(4), 489-499. <https://doi.org/10.1046/j.1440-0952.2001.00882.x>
- Ferry, J. M., & Watson, E. B. (2007). New thermodynamic models and revised calibrations for the ti-in-zircon and zr-in-rutile thermometers. *Contributions to Mineralogy and Petrology*, 154(4), 429-437.
- Hoskin, P. W., & Schaltegger, U. (2003). The composition of zircon and igneous and metamorphic petrogenesis. *Reviews in Mineralogy and Geochemistry*, 53(1), 27-62.
- Li, S., Miller, C. F., Tao, W., Xiao, W., & Chew, D. (2021). Role of sediment in generating contemporaneous, diverse “type” granitoid magmas. *Geology*, 50, 427-431. <https://doi.org/10.1130/G49509.1>
- Liu, H., Mckenzie, N. R., Colleps, C. L., Chen, W., Ying, Y., & Stockli, L., et al (2022). Zircon isotope–trace element compositions track paleozoic–mesozoic slab dynamics and terrane accretion in southeast asia. *Earth and Planetary Science Letters*, 578, 117298. <https://doi.org/https://doi.org/10.1016/j.epsl.2021.117298>
- Loucks, R. R., Fiorentini, M. L., & Henríquez, G. J. (2020). New magmatic oxybarometer using trace elements in zircon. *Journal of Petrology*, 1-30. <https://doi.org/10.1093/petrology/egaa034>
- Paton, C., Hellstrom, J., Paul, B., Woodhead, J., & Hergt, J. (2011). Iolite: freeware for the visualisation and processing of mass spectrometric data. *Journal of Analytical Atomic Spectrometry*, 26(12), 2508. <https://doi.org/10.1039/c1ja10172b>
- Tang, M., Ji, W., Chu, X., Wu, A., & Chen, C. (2020). Reconstructing crustal thickness evolution from europium anomalies in detrital zircons. *Geology*, 49 <https://doi.org/https://doi.org/10.1130/G47745.1>
- Vermeesch, P. (2021). On the treatment of discordant detrital zircon u–pb data. *Geochronology*, 3(1), 247-257. <https://doi.org/10.5194/gchron-3-247-2021>
- Xiang, D., Zhang, Z., Chew, D., Jolivet, M., Malusà, M. G., & Guo, C., et al (2023). Mesozoic-cenozoic topographic evolution of the south tianshan (NW china): insights from detrital apatite geo-thermochronological and geochemical analyses. *Lithosphere*, 190. [https://doi.org/10.2113/2023/lithosphere\\_2023\\_190/5953649/lithosphere\\_2023\\_190.pdf](https://doi.org/10.2113/2023/lithosphere_2023_190/5953649/lithosphere_2023_190.pdf)
- Zhu, Z., Campbell, I. H., Allen, C. M., & Burnham, A. D. (2020). S-type granites: their origin and distribution through time as determined from detrital zircons. *Earth and Planetary Science Letters*, 536, 116140. <https://doi.org/10.1016/j.epsl.2020.116140>